Journal of Structural Geology, Vol. 8, No. 7, pp. 737 to 752, 1986
Printed in Great Britain

0191-8141/86 $03.00 + 0.00
Pergamon Journals Ltd.

Fault geometries in basement-induced wrench faulting under different initial stress states

M. A. NAYLOR

Petroleum Development Oman LLC, Exploration Department, P.O. Box 81, Muscat, Sultanate of Oman

G. MANDL

Koninklijke/Shell Exploratie en Produktie Laboratorium, Volmerlaan 6, Rijswijk ZH, The Netherlands

and

C. H. K. SIJPESTEIJN

Brunei Shell Petroleum Co., Seria, Brunei

(*Received* 26 *March* 1985; *accepted in revised form* 3 *January* 1986)

Abstract—Scaled sandbox experiments were used to generate models for relative ages, dip, strike and three-dimensional shape of faults in basement-controlled wrench faulting. The basic fault sequence runs from early en échelon Riedel shears and splay faults through 'lower-angle' shears to P shears. The Riedel shears are concave upwards and define a tulip structure in cross-section. In three dimensions, each Riedel shear has a helicoidal form. The sequence of faults and three-dimensional geometry are rationalized in terms of the prevailing stress field and Coulomb–Mohr theory of shear failure. The stress state in the sedimentary overburden before wrenching begins has a substantial influence on the fault geometries and on the final complexity of the fault zone. With the maximum compressive stress (σ_1) initially parallel to the basement fault (transtension), Riedel shears are only slightly en échelon, sub-parallel to the basement fault, steeply dipping with a reduced helicoidal aspect. Conversely, with σ_1 initially perpendicular to the basement fault (transpression), Riedel shears are strongly oblique to the basement fault strike, have lower dips and an exaggerated helicoidal form; the final fault zone is both wide and complex. We find good agreement between the models and both mechanical theory and natural examples of wrench faulting.

INTRODUCTION

THE MOST varied styles of faulting are probably those induced in a lithified sedimentary sequence by transcurrent movements on an underlying basement fault. The complexities can be attributed to three causes: (a) the en échelon nature of faults and folds associated with wrench tectonics, (b) complications due to components of reverse or normal dip-slip on the basement fault and (c) lateral offsets of basement wrench faults, which create local extensional or compressional structures (e.g. Rodgers 1980, Crowell 1974, Segall & Pollard 1980).

A prerequisite for full understanding of wrench fault assemblages is a set of models for faults in a sedimentary overburden above a single basement wrench fault. We integrate scaled model experiments, mechanical theory and natural examples. We describe for the first time: (a) the sequence of faults in unconsolidated sand models, (b) their cross-sectional and three-dimensional geometry and (c) the important role of initial stress state in modifying the fault patterns.

Our experiments emphasize the process of faulting whilst neglecting, for example, folding, the role of lithologic and mechanical layering and pre-existing planes of weakness in the sedimentary overburden. Despite such idealizations, we find the models essential in the recognition and accurate interpretation of wrench fault zones.

EXPERIMENTAL TECHNIQUE

Cloos (1928) and Riedel (1929) were amongst the first to employ clay-cake models of wrench faulting, followed by Wilcox *et al.* (1973), Rixon (1978) and the shear-box models of Tchalenko (1968). More recently, Bartlett *et al.* (1981) examined wrench faulting, with small high-pressure rock models. Only Emmons (1969) has published a very limited account on sandbox models.

Scaling

A full discussion of scaling is beyond the scope of this paper, but the account below suffices to justify our approach. Certain idealizations of reality are needed to model faulting in the brittle crust. We neglect continuous deformation by time-dependent processes such as viscous flow and creep, which may occur during folding and ductile behaviour.

To ensure correspondence between fault structures in the model and nature (the 'geological prototype'), scaling rules have to be satisfied (Hubbert 1937, 1951). These rules are derived from a mechanical theory applicable to faulting in both model and prototype. The stress limits for faulting, that is the formation of slip-type discontinuities, are described by Coulomb–Mohr frictional plastic behaviour, in which the yield strength $\tau_{max} = c + \sigma_n \tan \phi$ (where c = cohesive strength,

σ_n = normal stress and ϕ = angle of internal friction).

Dry sand is a typical frictional plastic material, and its use has a long and respected history in soil mechanical and geological modelling (e.g. Hubbert 1951, Sanford 1959). Horsfield (1977) has shown that use of dry sand allows proper downscaling of frictional strength of natural rocks; stresses are scaled in the ratio of the length dimensions of the model and prototype. However, use of sand neglects the effect of cohesive strength (c) in the geological prototype, because c is practically zero in dry sand.

Clay models have the apparent advantage of generating folds and faults, but do not properly scale the yield strength (τ_{max}) of brittle rocks for two reasons. Firstly, the cohesive strength of clay, when scaled up to geological units several kilometres thick, implies very high cohesive strengths of natural rock. Secondly, the short duration of an experiment may not allow water in the clay to drain out under increased normal loads. In such undrained deformation, the effective confining pressure (total pressure minus fluid pressure) remains unchanged; the frictional component of yield strength is thus constant and not dependent on confining pressure. Clay will thus model the behaviour of rocks without pressure dependence of yield strength, and with a high cohesive strength. Such rocks will show highly ductile behaviour before faulting.

We conclude that whilst clay models may be applicable for the ductile lower crust, sand models are more appropriate to faulting in sedimentary rocks of the brittle upper crust.

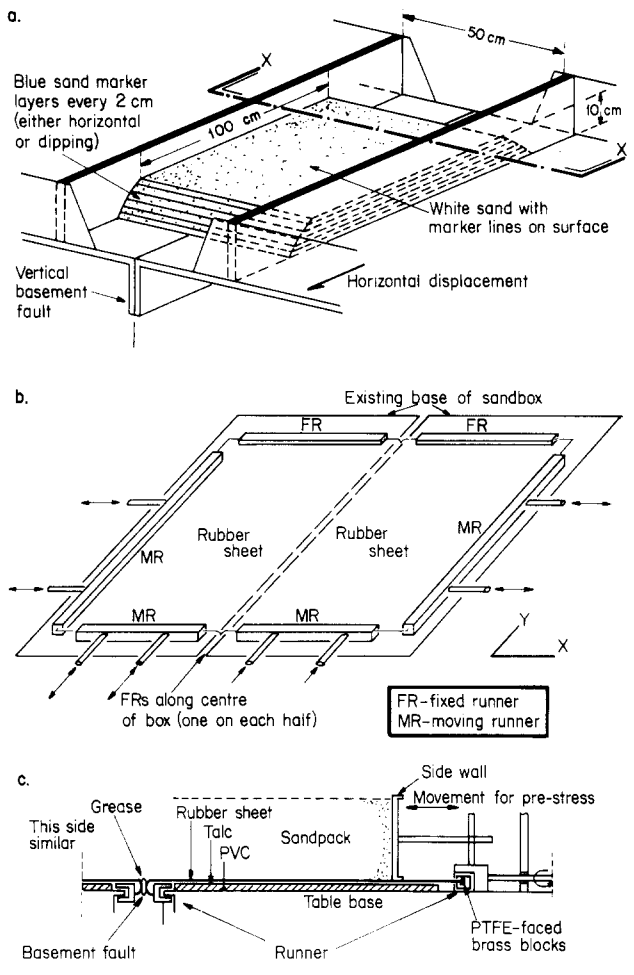

Fig. 1. (a) Sandbox used for wrench fault modelling. (b and c) Perspective and sectional views of the pre-stressing apparatus fitted to the sandbox. See text for discussion.

Operation of the sandbox

The sandbox used for wrench fault modelling is basically a table divided into two halves; one half of the table can be displaced laterally past the other by a motor drive, imitating movement on a single basement wrench fault (Fig. 1a). The rate at which the basement is displaced is a matter of experimental convenience since deformation is not dependent on strain rate in Coulomb–Mohr behaviour.

A pack of dry sand (grain size 0.15–0.3 mm), 10 cm thick, is deposited on the table from an overhead hopper moving to and fro on rails. This ensures a reproducible, uniform density in the pack. According to our scaling equation (Horsfield 1977), 10 cm of sand corresponds to 3 km of sediment resting on basement. Sand stained with methylene blue dye is used to make internal marker layers within the pack, and a grid of marker lines is created at the sandpack surface by sprinkling the dyed sand through a slotted stencil. Sandbox models have practical advantages over clay models in terms of reproducibility, ease and speed of preparation and in analysis of completed experiments.

Inspection of results

Photographs of the evolving experiment are taken at regular intervals with an overhead camera. Oblique illumination aids recognition of the faults which are manifested as brighter or darker surface escarpments and as offsets of marker lines. Selected completed experiments were impregnated with a dilute gelatin solution. The cohesion thus gained by the sand allows closely spaced (5 mm apart) horizontal or vertical serial sections to be made. Because fluid imbibes less into the dilated shear zones (faults) than into the unsheared material, faults are visible as lighter coloured zones of unwetted sand, as well as by small offsets of the marker layers.

Pre-stressing the sandpack

In order to apply a stress state other than that which results from sedimentation of the sandpack, a modification to the sandbox is needed. This consists of two rubber sheets, one fixed to each half of the sandbox by runners (Figs. 1b & c). For each table-half, two of the runners were fixed (at the centre-line and at one end), the other two being moved inwards and outwards using a crank, chain drives and threaded axles. With this apparatus, it is possible to stretch or relax the rubber sheet in directions parallel and perpendicular to the basement fault. For example, to apply an initial stress to

the overburden with σ_1 (maximum compressive stress) parallel to the basement fault and σ_3 (minimum principal stress) perpendicular to the basement fault, we would proceed as follows: (1) stretch the rubber in the direction parallel to the basement fault; (2) deposit the sandpack in the usual way and (3) allow the rubber to shorten in the direction parallel to the basement fault, at the same time applying a smaller extension in the perpendicular direction. A number of trials are required to determine the shortening and extension needed to give the required stress state without forming faults which could influence the course of the wrench experiment.

EVOLUTION OF A WRENCH ZONE: NO PRE-STRESSES

Experimental results

The evolution of experimental wrench fault zones has been discussed by several authors (e.g. Cloos 1928, Riedel 1929, Tchalenko 1968, Wilcox *et al.* 1973, Bartlett *et al.* 1981). Our results are largely compatible with their descriptions. With increasing basement displacement, the faults developing at surface are (Table 1, Case A, Fig. 2):

(1) *En échelon Riedel shears.* Their average strike is at 17° to the basement fault. The shears have lengths of 1 to 2 times the overburden thickness and overlap slightly with one another. Each shear is a 'scissor fault': its sense of vertical displacement reverses at its mid-point (where it crosses the basement fault). The region between two Riedels is always an up-squeezed block (Fig. 3a).

(2) *Short-lived splay faults.* These faults develop at or near the tips of Riedel shears, and strike at more than 17° to the basement fault.

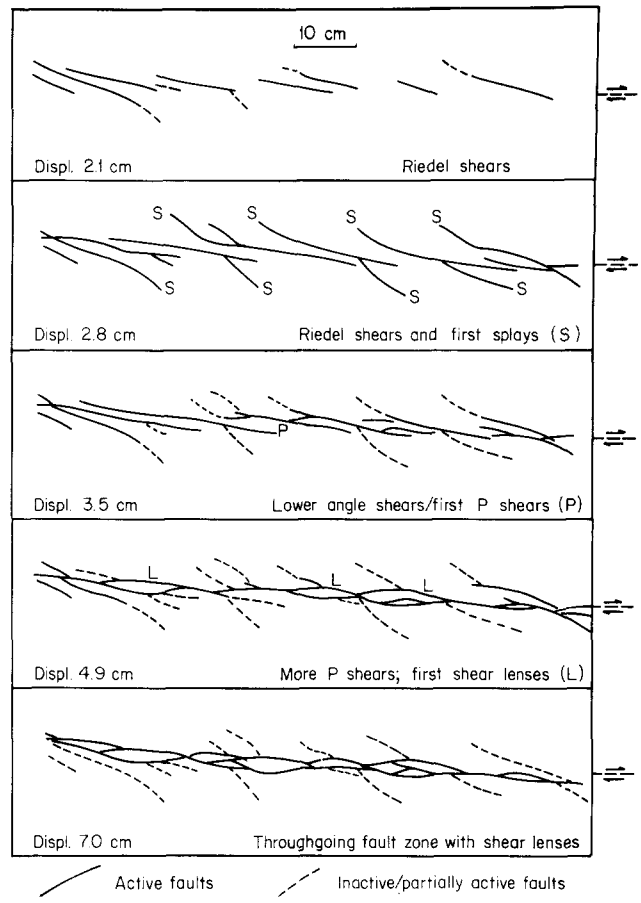

Fig. 2. Plan views drawn from photographs showing the evolution of an experimental wrench fault zone. Sandpack is 10 cm thick; no pre-stress applied.

Table 1. Summary of the characteristics of faults formed in the wrench fault experiments under different initial stress states

		Case A	Case B	Case C
		No pre-stress	σ_{Hmax} parallel to basement fault	σ_{Hmax} perpendicular to basement fault
Strike of first Riedels (1)	Mean	17	05	37
	95% are <	30	14	50
Dip at surface (degrees)	Mean	86	83	75
	95% are >	75	70	45
	Range	64–90	61–90	41–90
Dip at basement (degrees)	Mean	77	83	63
	95% are >	65	70	35
	Range	50–90	64–90	20–90
Displacement (2)	37° Riedel	—	—	0.3*
	17° Riedel	0.15*	—	0.4
	0° Riedel	0.25	0.1*	0.8
	Complete zone	0.35	0.2	0.8
Surface width of fault zone (2)		1.0	0.4	2.1
Length of first Riedels (2)		1.6	1.6	3.6
			4.1+	

(1) Strike in degrees, measured with respect to basement-fault direction. These are apparent dips (in degrees) seen in vertical sections perpendicular to the basement fault. Corrections to true dip are generally minimal (see text).

(2) Measured as fraction of overburden thickness.

*, indicates first fault to form; —, indicates this fault type not formed and +, for slightly en échelon and a single sinuous or straight fault.

(3) *Lower-angle shears* (striking at <17°). These shears develop when the splays are inactive, either from the tips of Riedel or splay faults or entirely between two Riedels. Antithetic Riedel shears (Fig. 4a), striking at ~72° to the basement fault, and with an opposite sense of shear to the Riedels, are only occasionally developed; their development is dependent on there being a substantial overlap between adjacent Riedel shears.

(4) *P shears*. These shears are occasionally formed; they have the same sense of shear displacement as the Riedels but cross the basement fault in the opposite direction (ideally at −15° to the basement fault). The lower-angle shears and P shears connect the discontinuous Riedel shears.

The final fault pattern is thus an anastomosing zone of faults defining shear lenses, with the displacement being concentrated on the central throughgoing faults.

Experiments with different sandpack thicknesses show that the Riedel shear lengths can be used to determine the approximate depth of sediment overlying basement (Table 1). The stage reached by a fault pattern is indicative of the total basement displacement, expressed in units of overburden thickness (Table 1, Fig. 2).

Significance of Riedel shears

During simple shear of a frictional plastic material, σ_1 attains an orientation at 45° to the imposed shear direction (Mandl *et al.* 1977). However, frictional plastic material tends to deform according to the Coulomb–Mohr slip concept (e.g. Jaeger & Cook 1976), faults being oriented at $45° - \phi/2$ to σ_1. Riedel shears are Coulomb–Mohr faults, at least at the free surface where σ_1 and σ_3 are horizontal. Densely packed sand has an angle of internal friction (ϕ) of 35–40°, which implies that the angle between a shear and σ_1 should be 28–25°, or that the shear strikes at 17–20° to the basement fault, as observed (Fig. 4a, Table 1).

Significance of later faults

The surface strikes of these faults also fit a Coulomb–Mohr slip model. We consider splay faults, lower-angle shears and P shears as due to modification of the initial stress field. At the tip of a fault, stresses will be re-oriented as indicated schematically in Fig. 4(b). On the extensional side of the fault tip, σ_1 will swing into orientations striking at >45° to the basement fault, and in addition the mean stress will be reduced. Faults will form readily under such conditions [cf. the active state of soil mechanics, e.g. Terzaghi (1966)]. The experimental splay faults are of this type and form consistently on the extensional side of the tip of a Riedel shear. They are short lived for kinematic reasons: their orientation is not suitable to take up large displacements imposed by the basement shear.

Similarly, the discontinuous Riedel shears are incapable of taking up all the basement displacement; interconnecting faults are clearly needed. On the compressional side of the Riedel shear tip, and more generally between two overlapping Riedel shears, σ_1 will be rotated towards the Riedel shear direction. Faults formed in this stress field will thus strike at <17° to the basement fault. The maximum stress rotation would occur if the Riedel shears were planes of no shear stress, when σ_1 would be parallel to the Riedels. P shears striking at ~15° to the basement fault closely approach this condition.

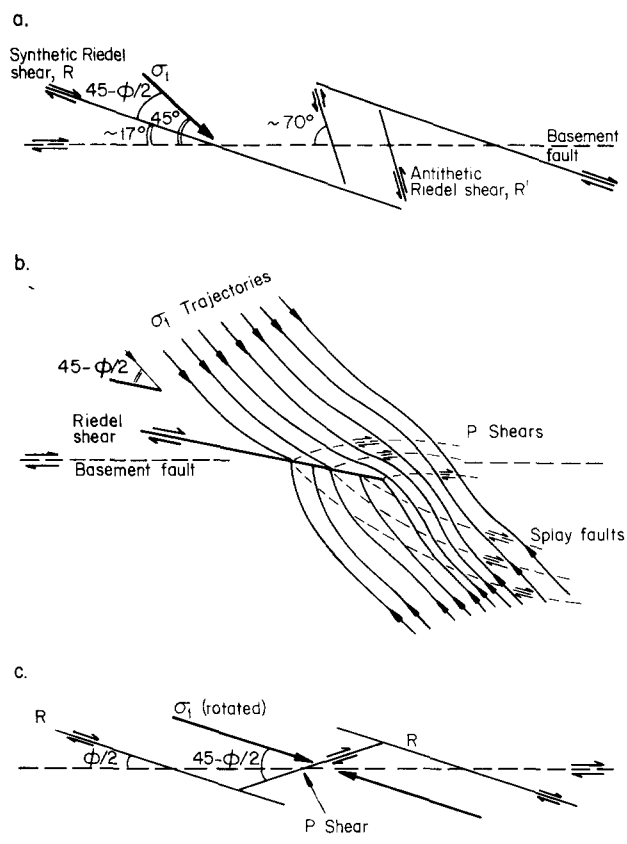

Fig. 4. Mechanical basis for the observed wrench fault pattern. (a) Riedel shears developed as Coulomb slip planes, σ_1 oriented at 45° to the basement fault strike. (b) Stress re-orientation on the compressional and extensional sides of the tip of a Riedel shear, showing potential secondary faults. (c) Stress re-orientation between two Riedel shears, generating lower-angle Riedel shears or P shears.

Discussion

High-pressure experiments with rock models do not predict identical development of a wrench zone (Bartlett *et al.* 1981). Riedels and P shears develop (almost) simultaneously (Table 2). This difference is attributed to

Table 2. Sequence of active faults in different wrench fault models

Sandbox models (this study)	Clay models (e.g. Wilcox *et al.* 1973)	Rock models (Bartlett *et al.* 1981)
R	R, R'	R, P
R, S	—	—
R, Y	(R')	R, P: X, R'
R, Y, P	(R, P), Y	Y

R, synthetic Riedel shear; R', antithetic Riedel shear; S, splay fault; Y, Y shear (= lower angle Riedel shear of this paper) parallel to basement fault and X, X shear, perpendicular to basement fault.

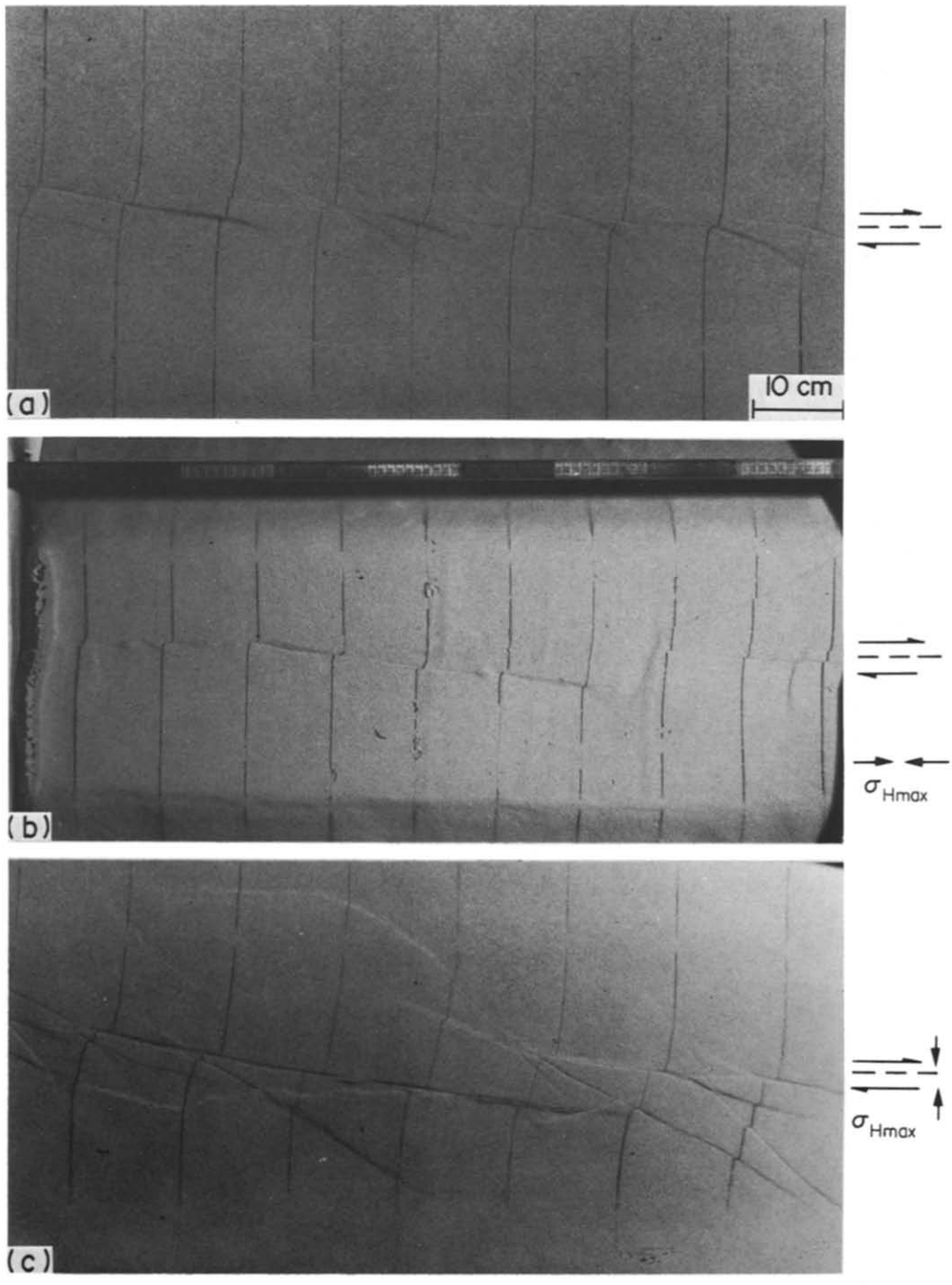

Fig. 3. Photographs showing typical Riedel shear patterns in the three types of experiment. (a) Case A, no pre-stress (as in Fig. 2). (b) Case B, sandpack pre-stressed with σ_1 parallel to the basement fault. (c) Case C, sandpack pre-stressed with σ_1 perpendicular to the basement fault. In all cases, sandpack is 10 cm thick and illumination is from the northern (top) side of the picture.

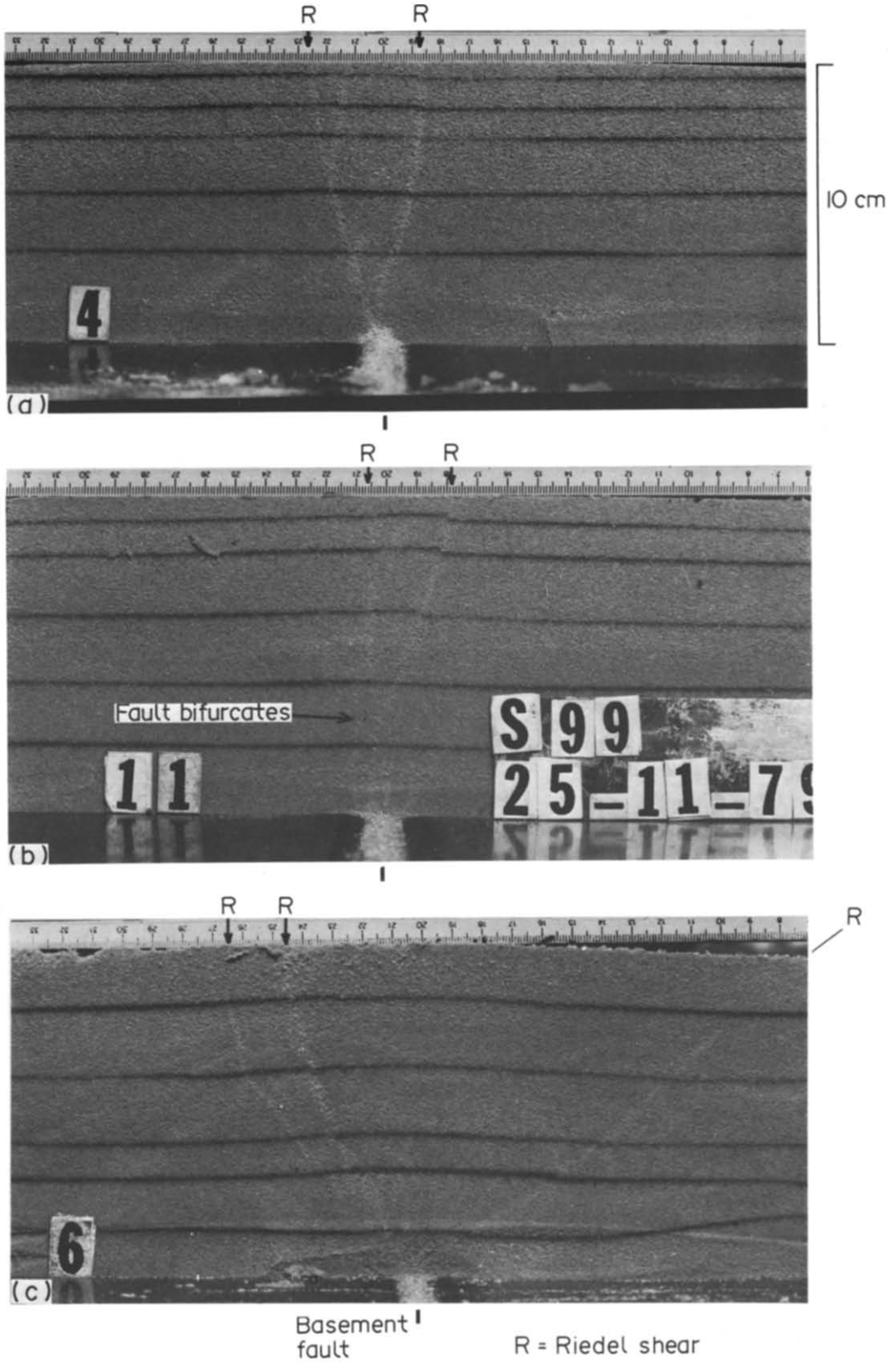

Fig. 6. Typical cross-sectional views of experimental Riedel shears, after impregnation and slicing of the sandpack. (a, b and c) correspond to the three stress states shown in Fig. 3.

the far greater elastic stiffness of limestone compared with sand; limestone will accommodate very limited displacements on Riedel shears before P shears have to form. The X shears in Bartlett's experiment may be rotated antithetic Riedel shears (cf. Mandl in press), post-peak strength faults allowing shear under reduced load (Bartlett *et al.* 1981). The Y shears in these experiments, and principal displacement shears in clay models are equivalent kinematically to our lower-angle Riedel shears, the late developed faults allowing development of a throughgoing fault zone.

It may be noted that experiments, and our analysis of stresses during wrench faulting, predict only two types of faults after Riedel shears: splay faults and lower-angle shears (including P shears). These two types, amongst several others of doubtful significance were predicted by Chinnery (1966a, b) in a more sophisticated, but no more physically appropriate, model of elastic dislocation theory.

Wrench faults in nature

The examples shown in Fig. 5 demonstrate the compatibility of the experimental results with natural cases of wrench faulting. En échelon fault patterns characterize the early stages of wrench and oblique-slip tectonics on various scales (Figs. 5a & c), for example in the Najd fault zone, Saudi Arabia (Moore 1979), the Alpine fault, New Zealand (Bishop 1968), the Fitzroy Trough, Australia (Smith 1968), the Dasht-e-Bayaz fault, Iran (Tchalenko & Ambraseys 1970, Tchalenko 1970), the faults of Shikoku Island, Japan (Kaneko 1966), the Newport–Inglewood trend, California (Wilcox *et al.* 1973), the San Andreas fault (Sharp 1975), and the Dead Sea Rift (Garfunkel *et al.* 1981). In many field cases, wrenching does not progress beyond the first set of Riedel shears.

Scissor faults comparable with those in experiments include faults in the Taranaki graben, New Zealand (Pilaar & Wakefield 1978), the Seal Beach oilfield, California (California Division of Oil and Gas 1960) and the Highland Boundary Fault, Scotland (Anderson 1946).

Examples of splay faults (Fig. 5b) include the faulting in the Alès coal basin, France (Arthaud & Matte 1977), the Alpine fault, New Zealand (Chinnery 1966b), possibly the Craven Fault system of northern England (Anderson 1951) and the faults of Shetland (Flinn 1977).

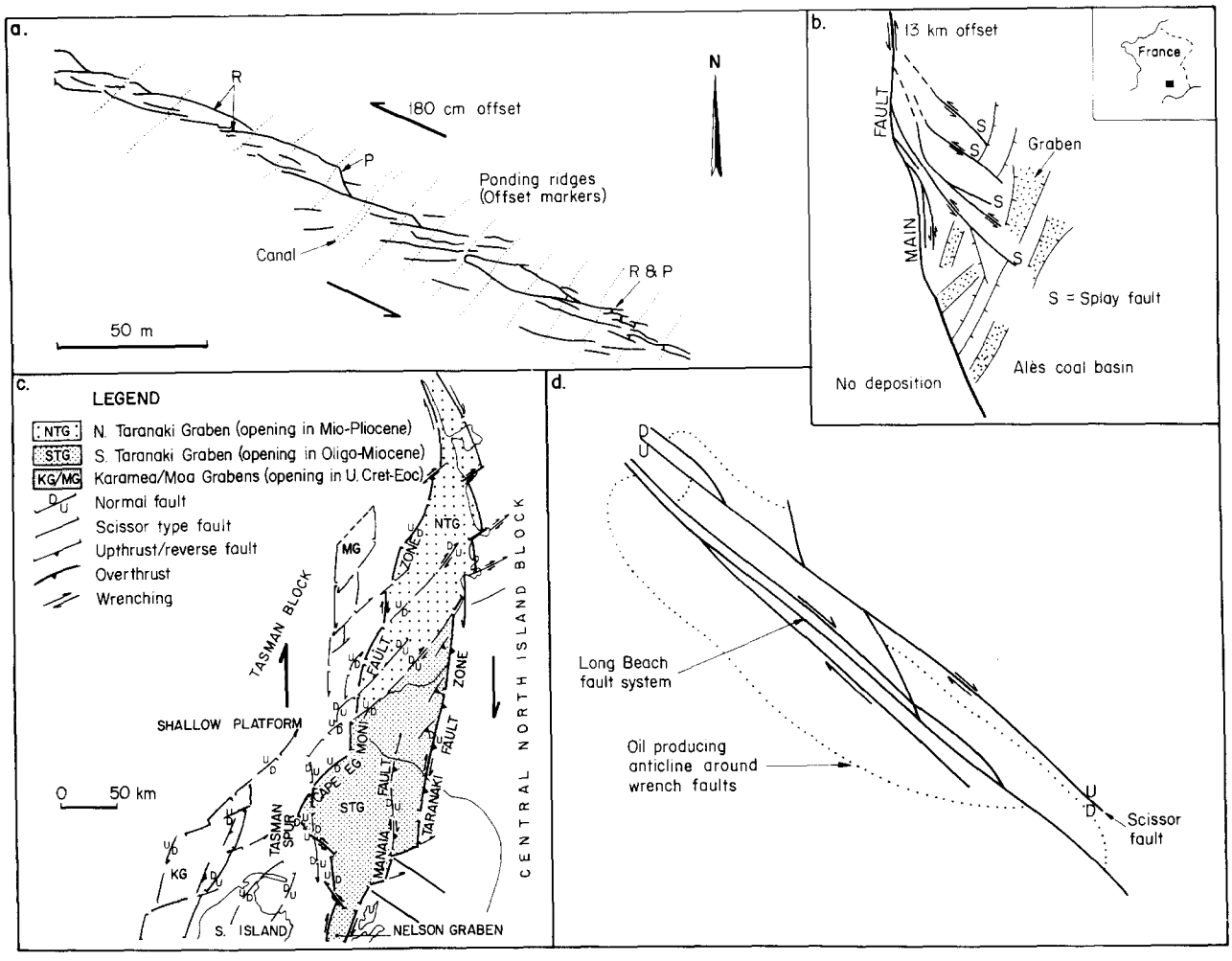

Fig. 5. Natural examples of wrench fault patterns. (a) Riedel and P shears in the Dasht-e-Bayaz fault zone, Iran (after Tchalenko 1970). (b) Splay faults in the Alès coal basin, France (after Arthaud & Matte 1977). (c) En échelon shears showing characteristic scissor faulting in the Taranaki graben, New Zealand, where wrenching post-dated graben formation (after Pilaar & Wakefield 1978). (d) Seal Beach oilfield, on the Newport–Inglewood trend, California (after California Division of Oil and Gas 1960).

The anastomosing faults typical of fully developed wrench systems are seen in, amongst others, the San Andreas fault system (Diblee 1968, Scholz 1977, Blake *et al.* 1978), the North Anatolian fault and the Dasht-e-Bayaz fault zone (Tchalenko 1970, fig. 5a). Anastomosing fault patterns are themselves often used as evidence for strike-slip faulting (e.g. Woodcock & Robertson 1982).

THREE-DIMENSIONAL GEOMETRY OF FAULTS

Riedel shears

A typical vertical section through the early stage of an experimental wrench zone (Fig. 6a) shows two concave-upwards Riedel shears, diverging from the basement fault, forming a 'tulip structure'. The shears have steep dips, typically 65° near the basement and 75–90° near the surface (Table 1). The degree of symmetry and width of the pattern depend primarily on the location of the section.

The three-dimensional geometries of many individual Riedel shears have been reconstructed from vertical and horizontal serial sections. Each shear has a helicoidal or 'plough-share' shape (Fig. 7a), which is a consequence of three factors: the en échelon nature of the shears at the surface, their concave-upwards geometry and the need to join a single basement fault at depth. The geometry of these shear faults is analogous to the form of en échelon tension cracks in small-scale shear zones (Wilson 1970, Pouba 1974, Knipe & White 1979, Pollard *et al.* 1982) and in glaciers (Meier 1960, Hambrey & Milnes, 1977). Of course, extension fractures are generally parallel to the local σ_1 direction, whereas shear faults are oriented at $45° - \phi/2$ to σ_1.

Reconstructions from serial sections indicate that each shear has the form of a parallelogram in lateral view (Fig. 7b). The terminations of faults are not vertical and may thus be seen to die out downwards or upwards in vertical sections. The horizontal displacement on a shear dies out towards its ends, where it is taken up by adjacent, overlapping faults.

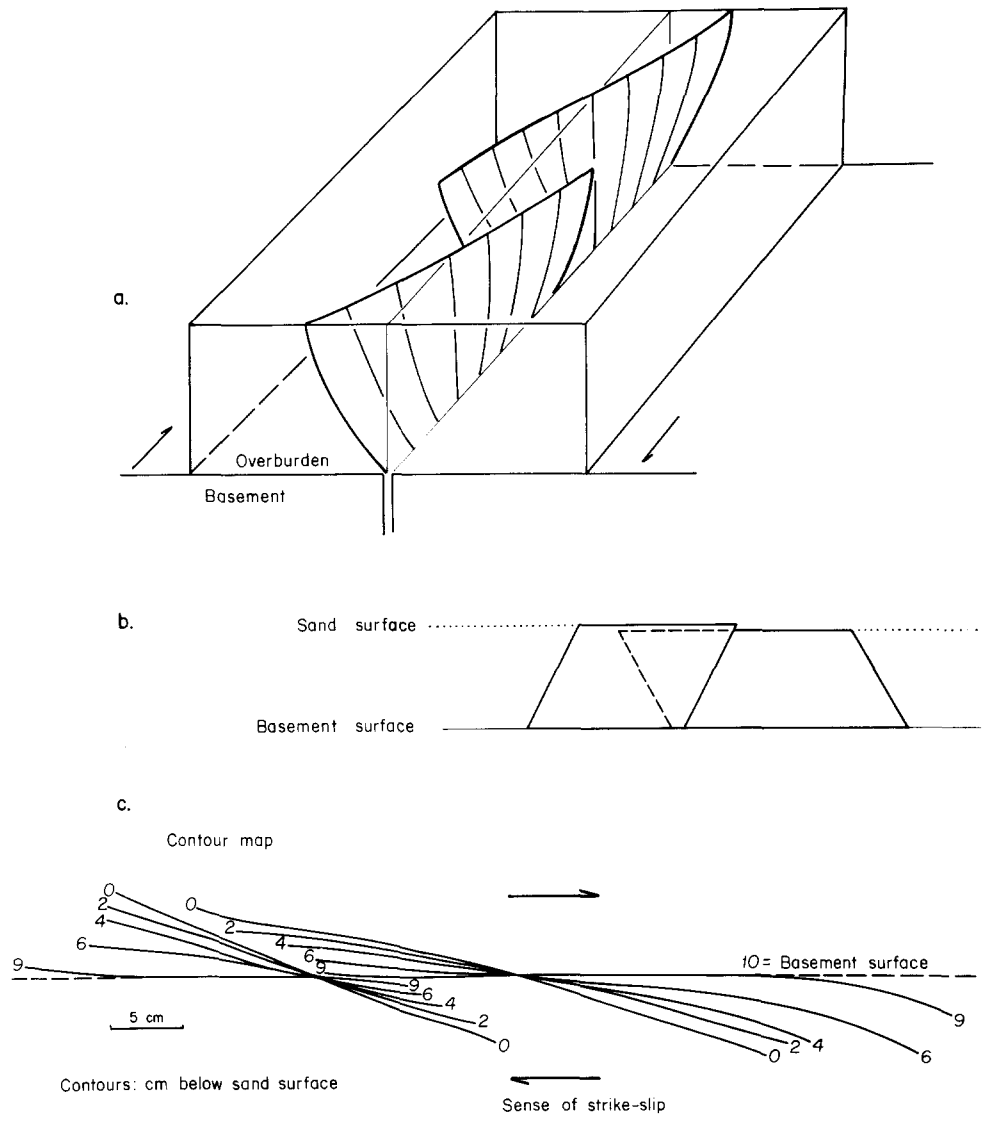

Fig. 7. (a) Helicoidal geometry of an individual Riedel shear, reconstructed from horizontal serial sections. (b) Schematic lateral view and (c) contour map, showing the parallelogram form of Riedel shears and their non-vertical terminations.

Mechanical significance of cross-sectional shape

Before wrench faulting begins, the horizontal normal stresses have equal magnitudes in all directions. Near the free surface, the shearing action of the basement will increase the horizontal stress at 45° to the basement fault, making it $\sigma_{H\,max}$ and eventually σ_1, the maximum compressive stress. The stresses in the subsurface will differ from these because of shear stresses ('drag') induced in the overburden by the strike-slip movement of the basement (Fig. 8a). These shear stresses are zero at the free surface and increase towards the basement. The resultant changes in σ_1 direction are shown schematically in Fig. 8(b).

The amount of stress rotation increases towards the basement fault; σ_1 rotates (a) towards parallelism with the vertical plane containing the basement fault strike and simultaneously (b) to a greater inclination with respect to the basement surface. Figure 8(b) indicates that Coulomb slip elements associated with these rotated directions define a concave-upwards form of Riedel shear.

Tulip or palm-tree structure?

Convex-upwards fault patterns, 'flower' or 'palm tree' structures, are commonly loosely attributed to wrench faulting (e.g. Lowell 1972, Sylvester & Smith 1976, Harding & Lowell 1979). Our experiments and the independent mechanical analysis (above) suggest that overburden wrench faults (Riedel shears) due to pure strike-slip basement movement are concave-upwards. This conclusion is borne out by natural examples, such as the Long Beach oilfield in California (Fig. 9b), faults in the Moray Firth, Scotland (Fig. 9a) (McQuillin *et al.*

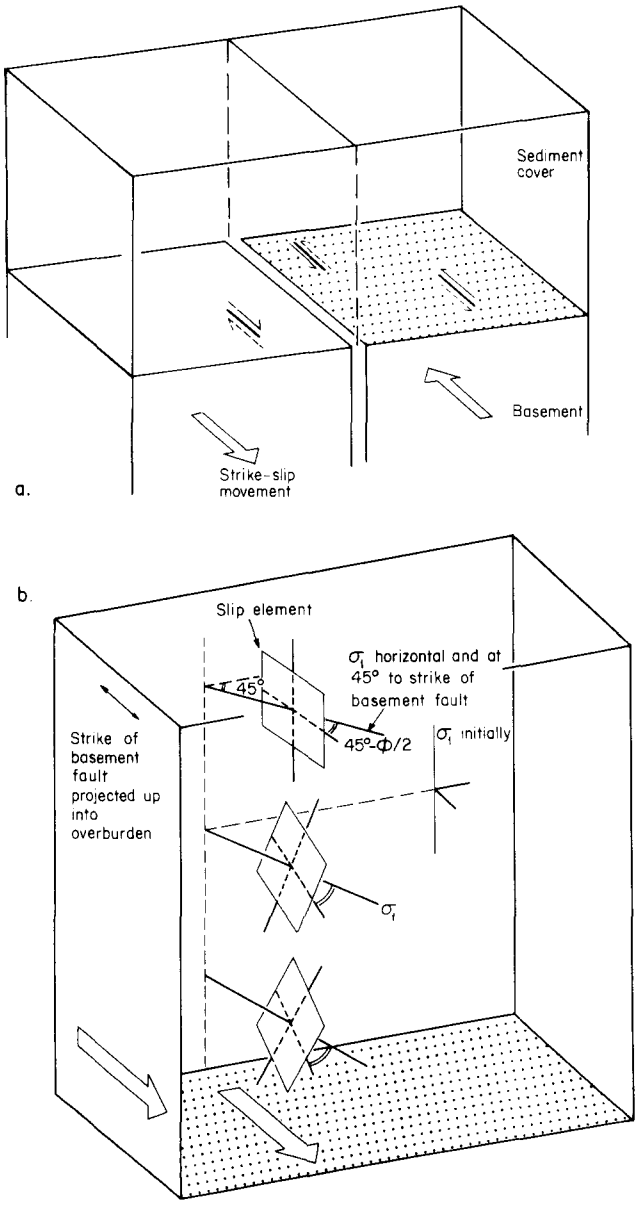

Fig. 8 (a) Shear stresses (shown as paired half-arrows) induced in the overburden by basement transcurrent movement. (b) Detail of part of the overburden in (a), showing the principal stress directions and associated Coulomb slip elements. See text for discussion.

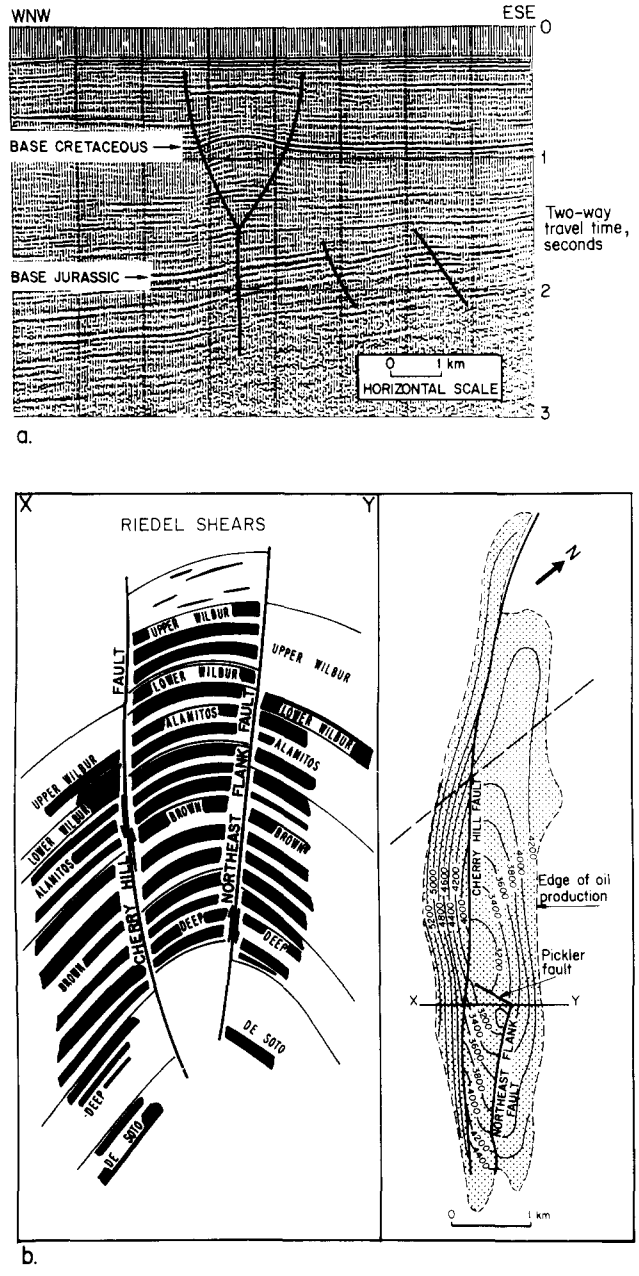

Fig. 9. Natural Riedel shears in cross-section. (a) Seismic line in the Moray Firth, Scotland; with permission of Shell U.K. Expro. (b) Long Beach oilfield, California (after California Division of Oil and Gas 1960).

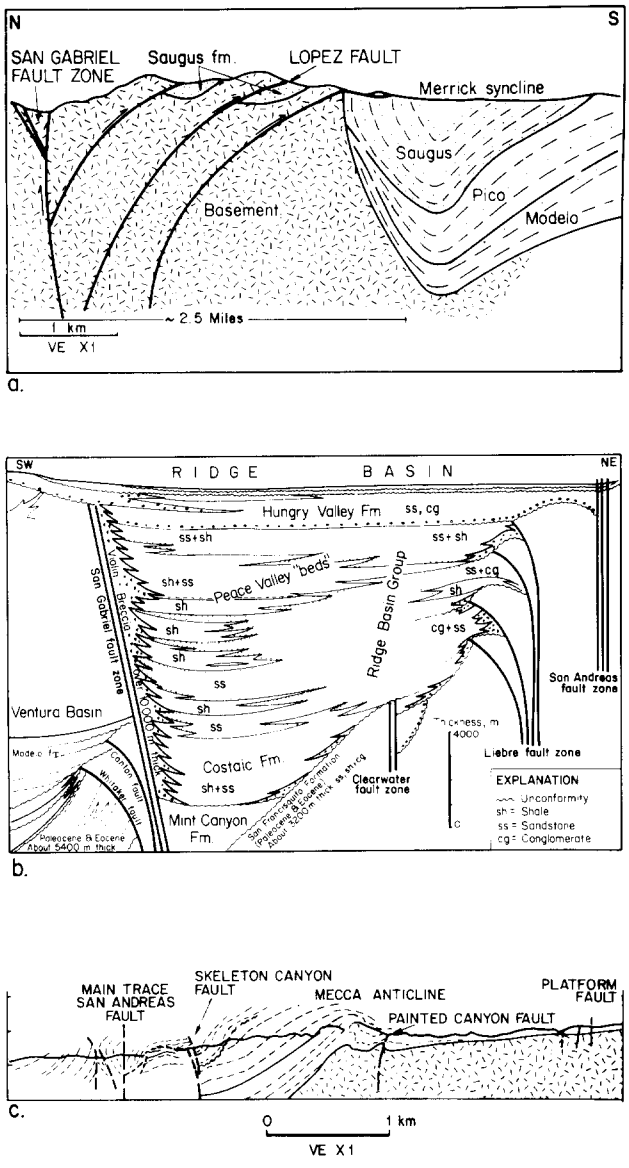

Fig. 10. Palm-tree structures related to oblique-slip tectonics in California. (a) San Gabriel fault zone, California (after Wilcox *et al.* 1973). (b) Liebre fault zone, Ridge Basin (Crowell 1976). (c) Mecca Hills (Sylvester & Smith 1976).

1982). Many examples seen on seismic sections are of the early stages of wrench faulting, comparable with simple Riedel shear patterns (Figs. 3a and 11a). Larger displacements result in complex fault zones which are generally beyond the resolution of seismic data.

We believe that convex-upwards faults in palm-tree structures are due primarily to oblique-slip faulting (combined dip-slip and strike-slip movement) on steeply dipping basement faults, particularly where the dip-slip component is a reverse displacement. Horsfield (1977) has shown that such dip-slip movements produce appropriately shaped, convex-upwards high-angle reverse faults. Furthermore, many natural palm tree structures made up of en échelon, apparently strike-slip faults have large components of dip-slip movement (Fig. 10) (Allen 1965, Wilcox *et al.* 1973, Crowell 1975, Sylvester & Smith 1976). In other cases, there may be ambiguity in interpreting the fault shapes from the available data (e.g. Harding 1985). Here, the use of models and correct identification of pure strike slip or oblique slip is important.

Variations in Riedel shear patterns

The 'model' Riedel shear geometry, often observed in experiments, gives an insight into the stresses associated with wrench faulting. A knowledge of the variations is needed to aid structural and seismic interpretation. Variations are of two types. (a) Variations in width and symmetry of the fault zone, and in dip of the faults (Fig. 11a) arise due to the position of the section with respect to the surface location of the Riedel shears. Near vertical Riedel shears, that is those sectioned near their mid-point, are commonly bowed with a 'sideways facing concavity'. (b) Kinks and feathering of Riedel shears (Fig. 11b) occur due to simultaneous initiation of shears at different levels in the overburden, such that segments do not coalesce to form a single smoothly curving fault. Kinked and branching faults may be more common in the lithologically heterogeneous overburdens of nature.

Splay faults, lower-angle shears and P shears

Splay faults initiate either smoothly or abruptly from Riedel shears, both in plan and cross section (Figs. 2 and 11c). The splays are relatively straight or slightly convex-upwards in section and have lower dips than the Riedel shears. In the case of a smooth transition, the fault changes from a steep concave-upwards Riedel into a flatter, straighter splay fault (Fig. 11). Splays may swing back into lower-angle shear, P-shear, or orientations, with the appropriate change of shape (see below), which contributes in plan view to the 'shear lens' structure of the fault zone.

Lower-angle Riedels and P shears, lying within the zone defined by the first Riedels, have steeper dips and a less pronounced helicoidal aspect than the Riedels. Near its mid-point, a P shear joins the basement fault directly, but tends to merge, towards its ends, at progressively higher levels with the bounding Riedel shears (Fig. 11d). Fault patterns similar to those shown in Fig. 11(d) are occasionally seen on seismic sections of exceptionally good definition.

ROLE OF INITIAL STRESS STATE

Rationale

Thus far, we have considered the simplest initial stress state (Case A, Table 1), with $\sigma_{H1} = \sigma_{H2} < \sigma_v$ (σ_{H1}, σ_{H2} are the two horizontal principal stresses; σ_v is the vertical principal stress). This state arises from sedimentation and uniaxial compaction of the laterally constrained sandpack. In such cases, $\sigma_{H1} = \sigma_{H2} = K_0 \sigma_v$, where K_0 is a constant less than unity (cf. Hafner 1951, Terzaghi 1966). This stress state may be applicable to certain 'undisturbed' sedimentary basins. However, there is abundant literature to suggest that (a) σ_H/σ_v can exceed

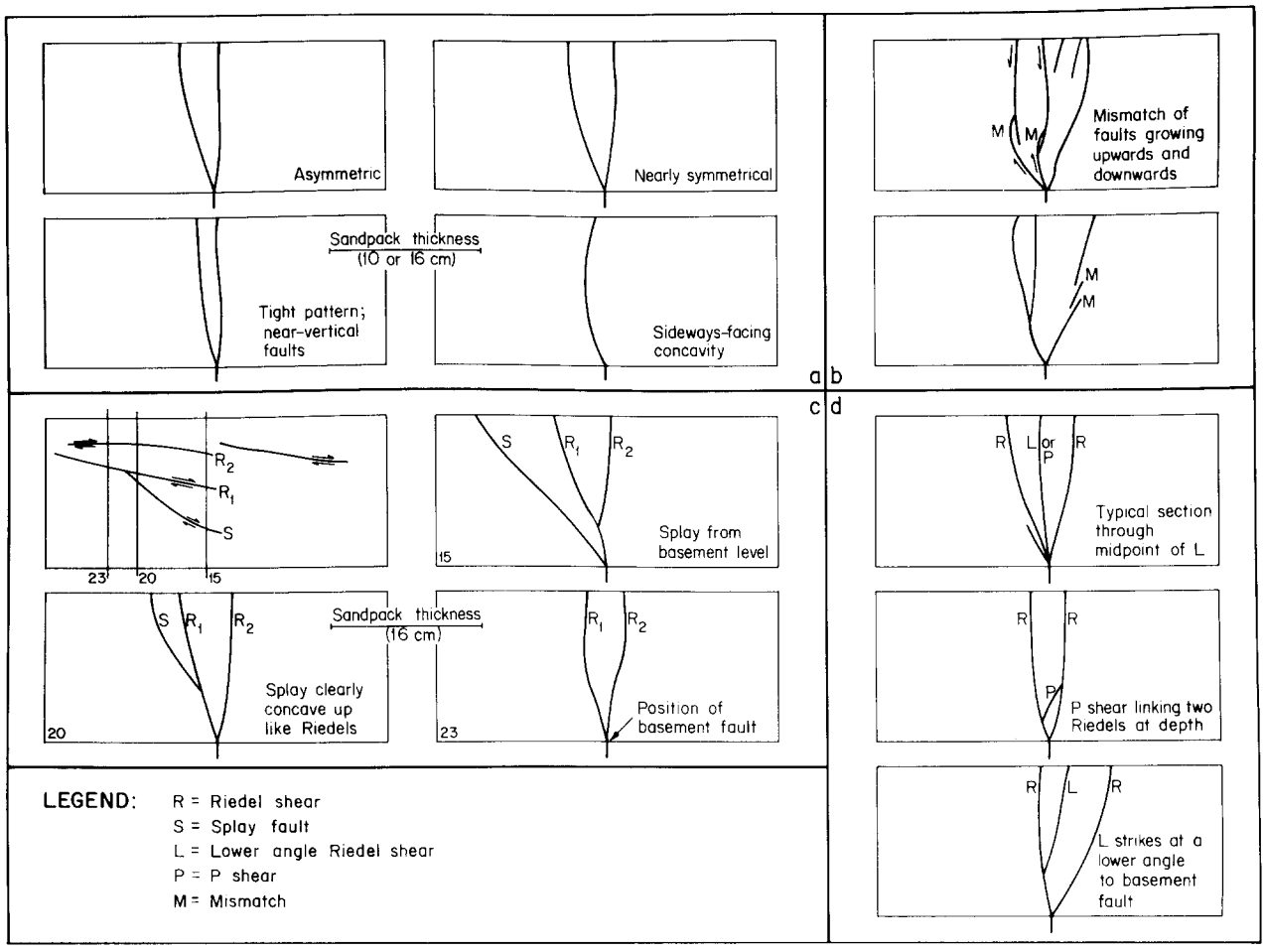

Fig. 11. Cross sections through experimental wrench fault zones (no pre-stress). (a) Variations in Riedel shear geometry due to location and spacing of shears with respect to section plane. (b) Kinks and feathering of Riedel shears, due to simultaneous initiation of non-matching fault segments at different levels in the sandpack. (c) Typical splay faults. (d) Geometries of lower-angle Riedel shears and P shears.

1 and (b) $\sigma_{H1} \neq \sigma_{H2}$ (Jamison & Cook 1980, Brown & Hoek 1978). Such variations in stress state are to be expected from such diverse effects as active tectonic stresses (e.g. Solomon *et al.* 1980), relict tectonic stresses from earlier deformation episodes, uplift and erosion (Voight 1966) and subsidence and/or uplift of non-circular sedimentary basins (Dallmus 1958, Price 1974).

In our experiments, two extreme cases were considered, each with $\sigma_{Hmin} < \sigma_v < \sigma_{Hmax}$ and with σ_1 parallel or perpendicular to the basement fault (Cases B and C, respectively, in Table 1). These stresses states were introduced in the sandpack using the pre-stressing apparatus described earlier. For simplicity, we describe models in which the stresses are applied before wrenching begins. Other experiments confirm that the results are essentially identical if the stressing and wrenching are simultaneous. We may therefore equate our Cases B and C with transtension (strike-slip plus extension) and transpression (strike-slip plus shortening), respectively.

Results with σ_{Hmax} parallel to the basement fault (Case B)

This stress state is characterized by the simplest and narrowest fault zone. En échelon Riedel shears are rare, but a single long wrench fault in the overburden is common. All faults are almost parallel to the basement fault (Figs. 3b and 12a). A throughgoing fault zone is generated after very small basement displacements (Table 1) and there is little tendency for an anastomosing fault zone with P shears to develop. The Riedels have steep dips, greater than 70°, and are almost straight in cross-section (Figs. 6b and 12b), where it is usual to see only one fault, or occasionally a fault bifurcating near surface into two weakly en échelon shears.

Results with σ_{Hmax} perpendicular to the basement fault (Case C)

A wide, complex fault zone results from wrench faulting with this initial stress state (Fig. 3c). The first en échelon Riedels strike at up to 60° (mean 37°) to the basement fault, and may swing round into reverse faults parallel to the basement fault. Increasing basement displacement generates shears at progressively smaller angles (as in Case A, Table 1) and the final braided fault zone may also contain P shears. In section (Figs. 3c and 13b) the faults have dips as low as 25° near basement and from 40 to 90° at surface (after correction for obliquity of section plane and dip direction). The helicoidal aspect of the Riedel shears is thus greatly exaggerated.

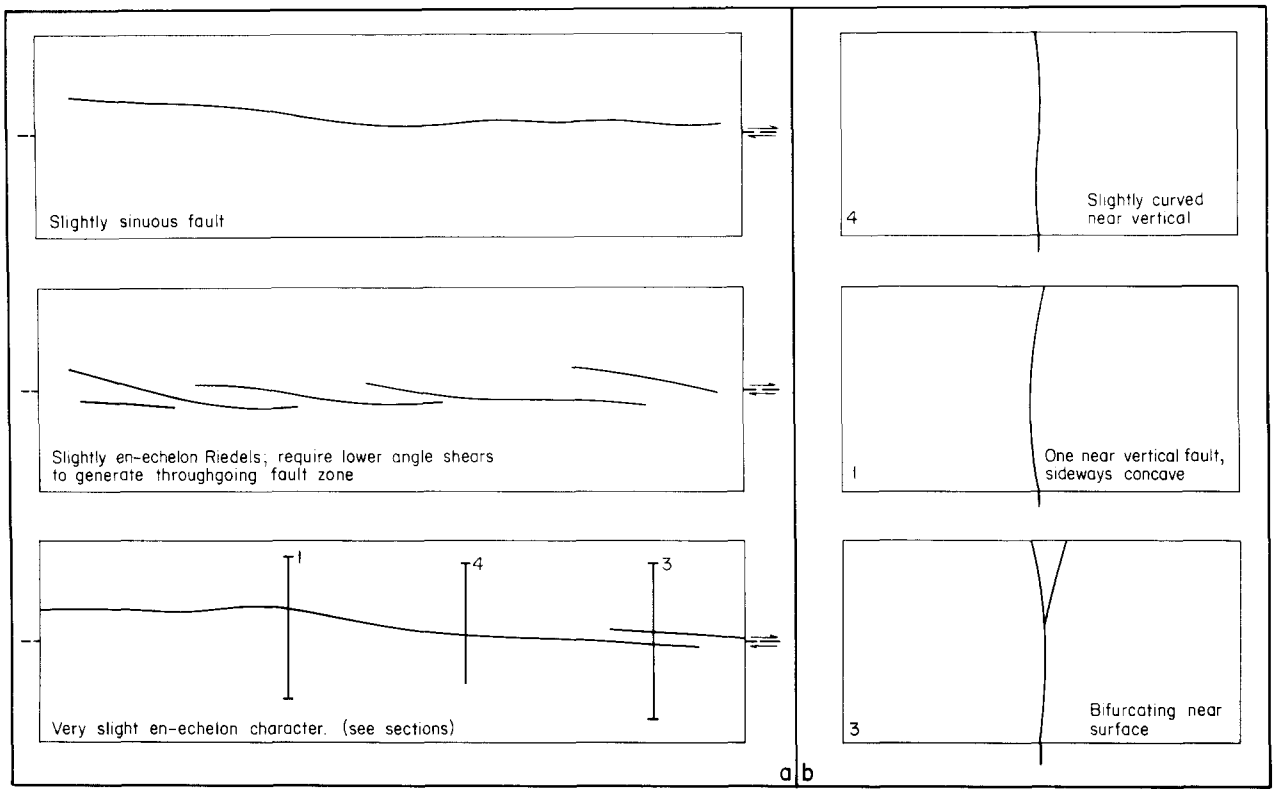

Fig. 12. Experimental results in Case B, pre-stressed with σ_1 parallel to the basement fault. (a) Typical plan views: small variations in strike and positions of early shears determine form of fully developed fault zone. (b) Typical cross-sectional views of the faults.

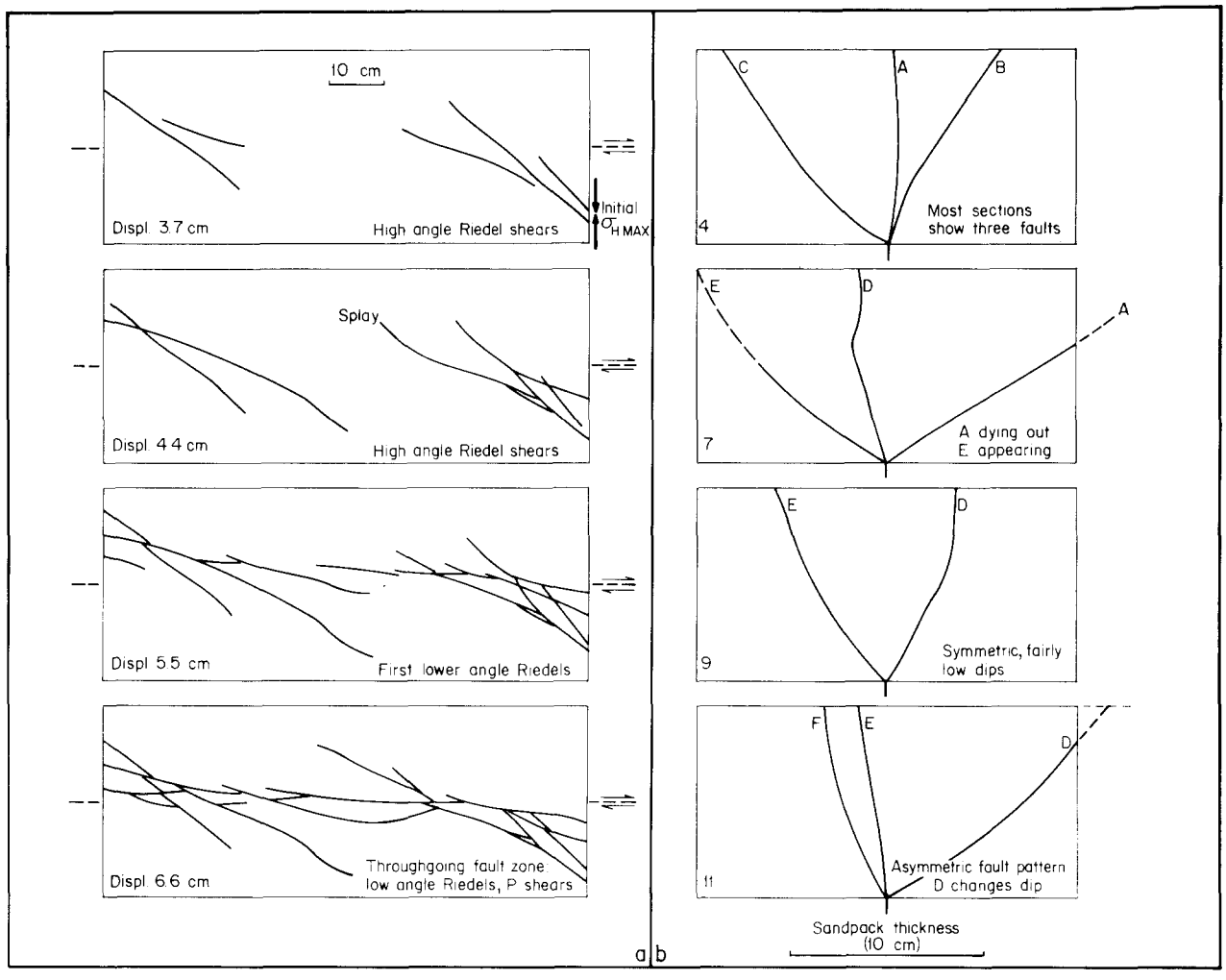

Fig. 13. Experimental results in Case C, pre-stressed with σ_1 perpendicular to the basement fault. (a) Evolution of the fault zone. (b) Series of sections from a separate experiment; sections are 10 cm apart.

Comparison of the three stress states

Salient observations from the three types of experiment are summarized in Table 1 (Cases A, B and C). Points of similarity include: (a) the en échelon character of the faults (in plan view); (b) development of a tulip structure with concave-upwards faults (in section) and (c) scissor faulting, in which the faults change their sense of throw along their length. It should be noted that these characteristics are only weakly developed in Case B (σ_{Hmax} initially parallel to the basement fault). Differences between the three cases lie in the dip and strike angles of the first Riedel shears, the complexity and width of the fully developed fault zone and the displacements required to generate a particular stage in the fault zone development.

Mechanical analysis

The strike orientation of the Riedel shears in the three initial stress cases can be explained as follows. In the case of no 'pre-stress', as already discussed, all horizontal normal stresses are initially equal (σ_3 undefined) and less than σ_v. Under the shear imposed by the basement movement, the horizontal stress at 45° to the basement fault immediately becomes σ_{Hmax} and eventually σ_1 (Fig. 14a), with its associated Riedel shears. In contrast, in the pre-stressed experiments, σ_1 is already defined, and must therefore *rotate* into the same 45° position. It appears that as σ_1 is rotating, differential stresses large enough to cause faulting arise. Thus in Case B, as σ_1 rotates from its initial position parallel to the basement fault, the Riedel shears which form will lie at a small angle to the basement fault (Fig. 14b). Furthermore, because these faults are almost parallel to the basement fault they are able to take up most or all of the applied displacement. As a result, few additional faults (if any) are formed as σ_1 continues rotating to the 45° position. In Case C, the first Riedel shears form as σ_1 rotates away from its initial position perpendicular to the basement fault (Fig. 14c). These faults thus strike at high angles to the basement fault, and are therefore kinematically able to accommodate little displacement. As σ_1 continues rotating, Riedel shears with smaller strike angles, and ultimately P shears have to form. These arguments, illustrated schematically in Fig. 14, can be shown more rigorously using the 'pole construction' on the Mohr stress circle.

From an entirely different, theoretical approach, using strain analysis, Sanderson & Marchini (1984) reached similar conclusions regarding the orientations of Riedel shears (their fig. 5). Under transtension (Case B), Riedels are subparallel to the shear direction (basement fault), and under transpression (Case C), they lie at high angles to the shear direction.

Natural examples

Despite the idealizations inherent in the experiments, we have found the models applicable in a number of situations where the initial stress field can be inferred from regional geological considerations.

An outstanding example of wrench faults formed with σ_{Hmax} initially (sub-) parallel to the basement wrench fault are the Icotea and La Paz–Mara faults in Venezuela. Regional tectonic synthesis shows a phase of E–W extension to have preceded wrench movements along an approximately N–S basement fault system. The Icotea fault, for example, is a scissor fault, which we consider to be a single Riedel shear more than 50 km long (Fig. 15a). It appears in cross section as a single fault, which changes dip along its length and therefore

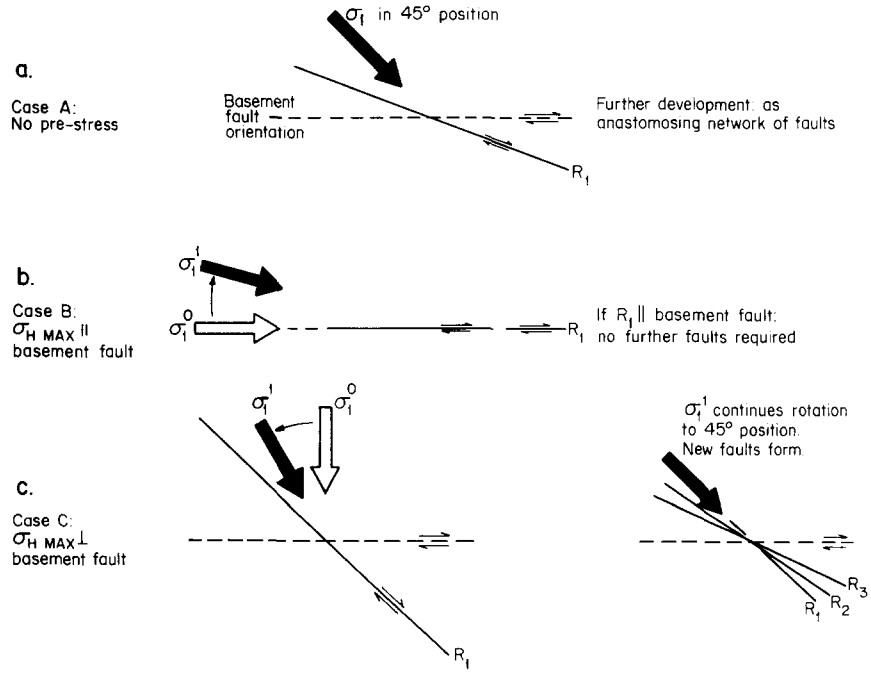

Fig. 14. Schematic explanation for the different Riedel shear orientations in the three experimental cases. (a) No pre-stress. (b) σ_{Hmax} parallel to basement fault. (c) σ_{Hmax} perpendicular to basement fault.

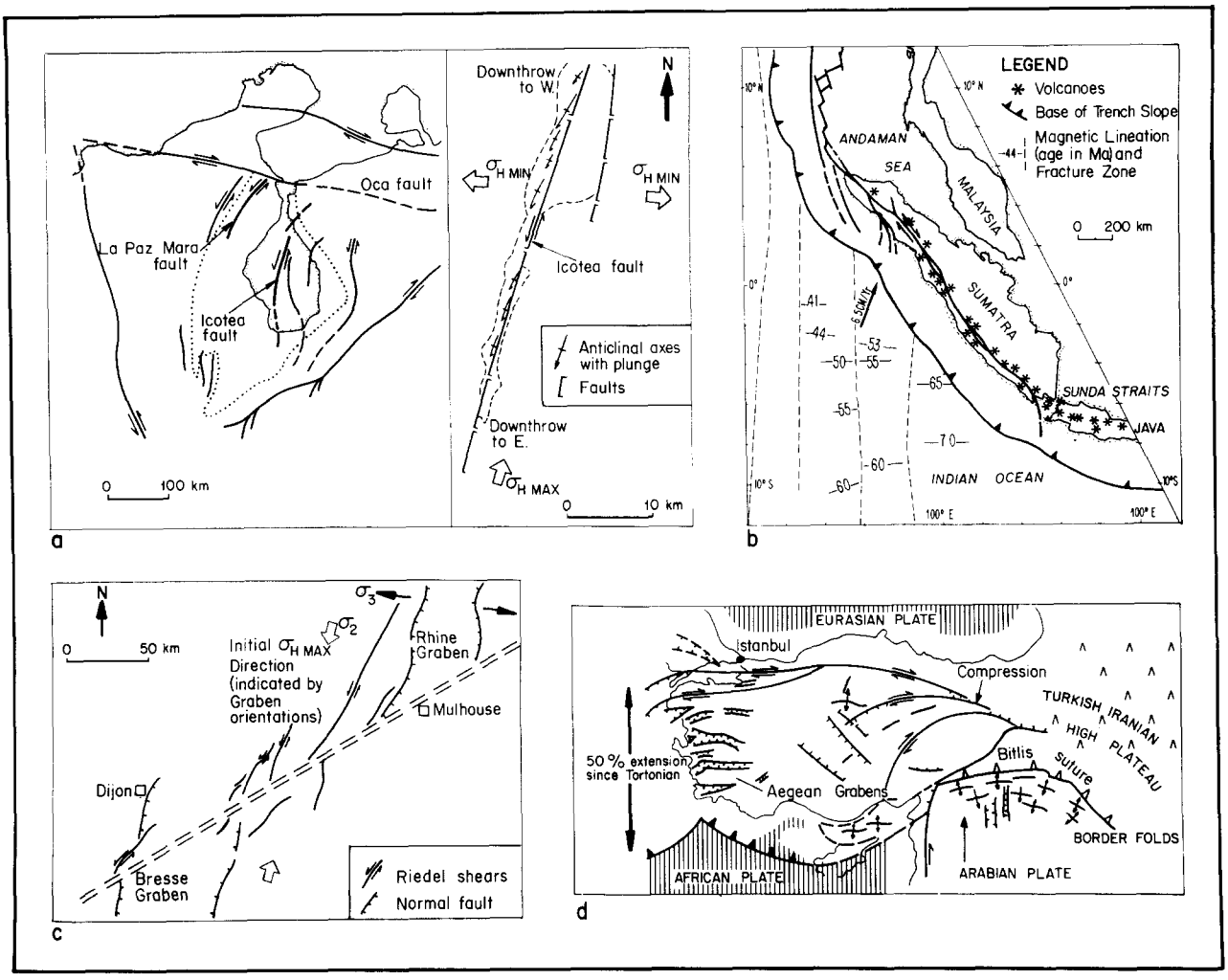

Fig. 15. Natural examples of wrench faults formed under different initial stress states. (a) Very simple pattern of long, straight, near vertical Riedel shears in the Icotea fault zone, Venezuela (σ_{Hmax} parallel to wrench zone): after Venezuela Studies Team (Shell, The Hague) with permission of Maraven. (b) 'High'-angle Riedel shears in an obliquely subducting plate boundary (σ_1 perpendicular to wrench zone) (after Karig *et al.* 1980). (c) Simplified sketch showing high-angle Riedel shears in the transform zone between the Rhine and Bresse grabens. (d) The Anatolian fault, Turkey, in Pliocene time (see text for discussion).

has a helicoidal form. In plan and cross-section, its simple geometry shows a strong resemblance to the appropriate experimental models (Figs. 3b, 6b and 12). Similarly, cross-sections through faults of the La Paz–Mara trend (Fig. 15a) are comparable with Fig. 3(b) with a single wrench fault bifurcating near surface.

Obliquely subducting plate boundaries commonly show adjacent parallel zones of thrusting and strike-slip tectonics (e.g. Fitch 1972, Lewis 1980), as well as (more distant) extensional tectonics in rear-arc spreading basins. One might expect that the shortening associated with the thrusting would have a pre-stressing effect such that σ_1 would be (sub-) perpendicular to the adjacent strike-slip zone, as in the experiments of Case C. This appears to be case; shears striking at high angles (>25°) to the throughgoing wrench zone are commonly developed, as illustrated in strands of the Zagros fault in Iran (Adamia *et al.* 1980). At the risk of oversimplification, the same appears to hold in the oblique subduction zone of Sumatra (Fig. 15b) where high-angle wrench fault strands cut the compressional part of the fore-arc.

The offset between the Rhine and Bresse grabens has been interpreted as a left-lateral transform zone separating the two rifts (Bergerat 1977). Since the grabens are parallel to the greater horizontal stress, σ_2, one may expect $\sigma_{H\,max}$ to have been initially perpendicular to the transform zone. This would account for the high angles between the Riedel faults and the transform zone (Fig. 15c).

A tectonic synthesis of Turkey (Sengor & Yilmaz 1981) may illustrate an example where both pre-stress states were active simultaneously. Sengor & Yilmaz postulate that the North Anatolian fault was a right lateral fault in Pliocene time, when Turkey was experiencing N–S extension in the western (Aegean) region and N–S compression due to microplate collision in the east. The 'initial' σ_{Hmax} orientations on the E–W North Anatolian fault were thus parallel and perpendicular to the fault in the west and east, respectively. In overall terms, this is in accord with the experimental models: in the west, a simple pattern of relatively straight faults with only slight en échelon character, and in the east, a complex system of faults striking at high angles to the trend of the zone (Fig. 15d).

CONCLUSIONS

(1) Basement controlled wrench faulting creates en échelon Riedel shears which have a helicoidal geometry, are concave upwards in cross section, and are scissor faults.

(2) The surface strike orientations of the early Riedel shears, and their dips are determined by the initial stress state (Table 1). For σ_{Hmax} parallel and perpendicular to the basement fault, the shears have respectively low and high strike angles and higher and lower dips. Popular representations of wrench fault orientation on a strain ellipse (e.g. Wilcox *et al.* 1973) are only valid for our Case A (no pre-stress).

(3) The width and complexity of the strike-slip zone is determined by the total basement displacement and by the initial stress state. The fault patterns are simplest and most complex for σ_{Hmax} initially parallel (transtension) and perpendicular (transpression) to the basement fault, respectively.

(4) The basement displacement required to generate the first faults at the surface is a small fraction of the overburden thickness and varies according to the initial stress state.

(5) After the first Riedel shears, further faults will develop unless the Riedel shears are parallel to the basement fault (as is the case when σ_{Hmax} is initially parallel to the basement fault). This development is characterized by short-lived splay faults at higher strike angles, and then by lower-angle Riedel shears and by P shears.

(6) Pure strike-slip displacements generate concave-upwards faults arranged in a tulip structure. Convex-upwards faults in the form of a palm-tree structure (when associated with an en échelon fault pattern in map view) are attributable to transpression or to combined strike-slip and dip-slip movements on steeply dipping basement faults.

(7) These models are of practical value in the interpretation (in cross-section and map) of often poorly defined wrench fault patterns seen on seismic sections in the uppermost few kilometres of the earth's crust.

Acknowledgements—This study was part of a research programme in wrench tectonics at the Koninklijke/Shell Exploratie en Produktie Laboratorium, Rijswijk. We thank Shell Research B.V. for permission to publish this paper, which benefited from discussions with many colleagues including J. Haremboure, W. T. Horsfield, S. Snelson and E. A. Haan. E. A. Haan and N. van Ooyen performed some of the experiments. C.H.K.S. did the experimental work as a part requirement for a master's thesis at the State University of Utrecht. M.A.N. thanks Shell Development Company, Houston for the opportunity to study wrench faults in California. We thank Shell UK Expro and Maraven for permission to use material in Figs. 9 and 15.

REFERENCES

Adamia, S., Bergougnan, H., Fourquic, C., Haghipour, A., Lordkipanidze, M., Ozgul, N., Ricou, L. E. & Zakariadze G. 1980. The Alphine Middle East between the Aegean and the Oman traverses. *Bur. Res. Geol. Min. Mem* **115**, 122–136 (Geology of the Alpine chains born of the Tethys. Colloquium C5, 26th Int. Geol. Congre., Paris, July 1980).

Allen, C. R. 1965. Transcurrent faults in continental areas. *Phil. Trans. R. Soc. Lond.* **A258**, 82–89.

Anderson, E. M. 1951. *The Dynamics of Faulting* (2nd Edn). Oliver & Boyd, Edinburgh.

Anderson, J. G. C. 1946. The geology of the Highland Border: Stonehaven to Arran. *Trans. R. Soc. Edin.* **61**, 479–515.

Arthaud, F. & Matte, Ph. 1977. Late Palaeozoic strike slip faulting in southern Europe and northern Africa: result of a right lateral shear zone between the Appalachians and the Urals. *Bull. geol. Soc. Am.* **88**, 1305–1320.

Bartlett, W. L., Friedman, M. & Logan, J. M. 1981. Experimental folding and faulting of rocks under confining pressure—IX. Wrench faults in limestone layers. *Tectonophysics* **79**, 255–277.

Bergerat, F. 1977. La fracturation de l'avant pays jurassien entre les fosses de la Saone et du Rhin; analyse et essai d'interpretation dynamique. *Revue Geogr. Physique Geol. Dynamique* Ser. 2 **24**, 325–338.

Bishop, D. G. 1968. The geometric relationship of structural features associated with major strike-slip faults in New Zealand. *N.Z. J. Geol. Geophys.* **11**, 405–417.

Blake, M. C., Campbell, R. H., Diblee, T. W., Jr., Howell, D. G., Normark, W. R., Vedder, J. C., Nilsen, T. H. & Silver, E. A. 1978. Neogene basin formation in relation to plate tectonic evolution of San Andreas fault system, California. *Bull. Am. Ass. Petrol. Geol.* **62**, 344–372.

Brown, E. T. & Hoek, E. 1978. Trends in relationships between measured in-situ stresses and depth. *Int. J. Rock. Mech. Mining. Sci. Geomech. Abstr.* **15**, 211–215.

California Division of Oil & Gas 1960. California oil and gas fields. Field maps and data sheets. Parts 1 and 2. San Francisco, October 1960.

Chinnery, M. A. 1966a. Secondary faulting—I. Theoretical aspects. *Can J. Earth Sci.* **3**, 163–174.

Chinnery, M. A. 1966b. Secondary faulting—II. Geological aspects. *Can J. Earth Sci.* **3**, 175–190.

Cloos, H. 1928. Experimenten zur Inneren Tektonik. *Centralbl f. Mineralogie 1928, Abt. B*, 609–621.

Crowell, J. C. 1974. Origin of late Cenozoic basins in southern California. In: *Tectonics and sedimentation* (edited by Dickinson, W. R.). *Soc. Econ. Paleont. Miner. Sp. Pub.* **22**, 190–204.

Crowell, J. C. 1975. The San Gabriel fault and Ridge Basin, Southern California. *Calif. Div. Mines Geol. Spec. Rep.* **118**, 208–219.

Dallmus, K. F. 1958. Mechanics of basin evolution and its relation to the habitat of oil in the basin. In: *Habitat of Oil* (edited by Weeks, L. G.). *Am. Ass. Petrol. Geol.*, Tulsa.

Diblee, T. W., Jr. 1968. Displacement of the San Andreas fault system in the San Gabriel Mountains, San Bernardino and San Jacinto Mountains, Southern California. In: *Proceedings of Conference on Geologic Problems of the San Andreas Fault System* (edited by Dickinson, W. R. & Grantz, A.). *Stanford Univ. School Earth Sci.* **11**, 260–278.

Emmons, R. C. 1969. Strike-slip rupture patterns in sand models. *Tectonophysics* **21**, 93–134.

Fitch, T. J. 1972. Plate convergence, transcurrent faults and internal deformation adjacent to southeast Asia and the Western Pacific. *J. geophys. Res.* **77**, 4432–4460.

Flinn, D. 1977. Transcurrent faults and associated cataclasis in Shetland. *J. geol. Soc. Lond.* **133**, 231–248.

Garfunkel, Z. Zak, I. & Freund, R. 1981. Active faulting in the Dead Sea rift. *Tectonophysics* **80**, 1–26.

Hafner, W. 1951. Stress distributions and faulting. *Bull. geol. Soc. Am.* **62**, 373–398.

Hambrey, M. J. & Milnes, A. G. 1977. Structural geology of an Alpine glacier (Griesgletscher, Valais, Switzerland). *Eclog. geol. Helv.* **70**, 667–684.

Harding, T. P. 1985. Seismic characteristics and identification of negative flower structures, positive flower structures and positive structural inversion. *Bull. Am. Ass. Petrol. Geol.* **69**, 582–600.

Harding, T. P. & Lowell, J. D. 1979. Structural styles, their plate tectonic habitats and hydrocarbon traps in petroleum provinces. *Bull. Am. Ass. Petrol. Geol.* **63**, 1016–1058.

Horsfield, W. T. 1977. An experimental approach to basement controlled faulting. In: *Fault Tectonics in NW Europe* (edited by Frost, R. T. C. & Dikkers, A. J.). *Geologie Mijnb.* **56**, 363–370.

Hubbert, M. K. 1937. Theory of scale models as applied to the study of geological structures. *Bull. geol. Soc. Am.* **48**, 1459–1520.

Hubbert, M. K. 1951. Mechanical basis for certain familiar geological structures. *Bull. geol. Soc. Am.* **62**, 355–372.

Jaeger, J. C. & Cook, N. G. W. 1976. *Fundamentals of Rock Mechanics*. John Wiley, New York.

Jamison, D. B. & Cook, N. G. W. 1980. Note on measured values for the state of stress in the earth's crust. *J. geophys. Res.* **85**, 1833–1838.

Kaneko, S. 1966. Transcurrent displacement along the Median Line, south western Japan. *N.Z. J. Geol. Geophys.* **9**, 45–59.

Karig, D., Lawrence, M. B., Moore, G. F. & Curray, J. R. 1980. Structural framework of the forearc basin, NW Sumatra. *J. geol. Soc. Lond.* **137**, 77–91.

Knipe, R. J. & White, S. H. 1979. Deformation in low grade shear zones in the Old Red Sandstone, SW Wales. *J. Struct. Geol.* **1**, 53–66.

Lewis, K. B. 1980. Quarternary sedimentation on the Hikurangi oblique subduction and transform margin. In: *Sedimentation in Oblique Slip Mobile Zones* (edited by Ballance, P. F. & Reading, H. G.). *Spec. Publ Int. Ass. Sediment* **4**, 171–189.

Lowell, J. D. 1972. Spitsbergen Tertiary orogenic belt and the Spitsbergen fracture zone. *Bull. geol. Soc. Am.* **83**, 3091–3102.

Mandl, G. (in press). Tectonic deformation by rotating parallel faults—'The bookshelf mechanism'. *Tectonophysics.*

Mandl, G., De Jong, L. N. J. & Maltha, A. 1977. Shear zones in granular material. *Rock Mech.* **9**, 95–144.

McQuillin, R., Donato, J. A. & Tulstrup, J. 1982. Development of basins in the Inner Moray Firth and the North Sea by crustal extension and dextral displacement of the Great Glen Fault. *Earth Planet. Sci. Lett.* **60**, 127–139.

Meier, M. F. 1960. Mode of flow of Saskatchewan glacier, Alberta, Canada. *U.S. Geol. Surv. Prov. Pap.* **351**, 1–70.

Moore, J. McM. 1979. Tectonics of the Najd transcurrent fault system, Saudi Arabia. *J. geol. Soc. Lond.* **136**, 441–452.

Pilaar, W. F. H. & Wakefield, L. L. 1978. Structural and stratigraphic evolution of the Taranaki basin, offshore North Island, New Zealand. *Austral. Petrol. Expl. Assoc. J.* **1978**, 93–101.

Pouba, Z. 1974. The function of en-echelon cracks. *Sbornik Geologickych Fed., Geologie* **26**, 125–133.

Pollard, D. D., Segall, P. & Delaney, P. T. 1982. Formation and interpretation of dilatant echelon cracks. *Bull. geol. Soc. Am.* **93**, 1291–1303.

Price, N. J. 1974. The development of stress systems and fracture patterns in undeformed sediments. *Proc. 3rd Int. Conf. Soc. Rock Mech.*, Denver, Colorado, **1A**, 487–498.

Riedel, W. 1929. Zur Mechanik geologischer Brucherscheinungen. *Zb. Miner. Geol. Palaeont. Abh. B*, 354–368.

Rixon, L. K. 1978. Clay modelling of the Fitzroy graben. *BMR J. Austral. Geol. Geophys.* **3**, 71–76.

Rodgers, D. A. 1980. Analysis of pull apart basin development produced by en echelon strike slip faults. In: *Sedimentation in Oblique Slip Mobile Zones* (edited by Ballance, P. F. & Reading, H. G.). *Spec. Publ Int. Ass. Sediment.* **4**, 27–41.

Sanderson, D. J. & Marchini W. R. D. 1984. Transpression. *J. Struct. Geol.* **6**, 449–458.

Sanford, A. R. 1959. Analytical and experimental study of simple geological structures. *Bull. geol. Soc. Am.* **70**, 19–52.

Scholz, C. H. 1977. Transform fault systems of California and New Zealand: similarities in their tectonic and seismic styles. *J. geol. Soc. Lond.* **133**, 215–229.

Segall, P. & Pollard, D. D. 1980. Mechanics of discontinuous faults. *J. geophys. Res.* **85**, 4337–4350.

Sengor, A. M. C. 1979. The North Anatolian transform fault: its age, offset, and tectonic significance. *J. geol. Soc. Lond.* **136**, 269–282.

Sengor, A. M. C. & Yilmaz, Y. 1981. Tethyan evolution of Turkey: a plate tectonic approach. *Tectonophysics* **75**, 181–241.

Seymin, I. & Aydin A. 1972. The Bingol earthquake and its relation to the North Anatolian fault zone. *Bull. Min. Res. Expl. Inst. Turkey* **79**, 1–8.

Sharp, R. V. 1975. En échelon fault patterns of the San Jacinto fault zone. *Calif. Div. Mines & Geol., Spec. Rep.* **118**, 147–152.

Smith, J. G. 1968. Tectonics of the Fitzroy wrench trough, western Australia. *Am. J. Sci.* **266**, 766–776.

Solomon, S. C., Richardson R. M. & Bergman, E. A. 1980. Tectonic stress: models and magnitudes. *J. geophys. Res.* **85**, 6086–6092.

Sylvester, A. G. & Smith, R. R. 1976. Tectonic transpression and basement controlled deformation in the San Andreas fault zone, Salton Trough California. *Bull. Am. Ass. Petrol. Geol.* **60**, 2081–2102.

Tchalenko, J. S. 1968. The evolution of kink-bands and the development of compressional textures in sheared clay. *Tectonophysics* **6**, 159–174.

Tchalenko, J. S. 1970. Similarities between shear zones of different magnitudes. *Bull. geol. Soc. Am.* **81**, 1625–1640.

Tchalenko, J. S. & Ambraseys, N. N. 1970. Structural analysis of the Dasht-e-Bayaz (Iran) earthquake fractures. *Bull. geol. Soc. Am.* **81**, 41–60.

Terzaghi, K. 1966. *Theoretical Soil Mechanics*. John Wiley, New York.

Voight, B. 1966. Restspannungen im Gestein. *Proc. 1st Int. Conf. Soc. Rock Mechanics*, Lisbon, 2.

Wilcox, R. E. Harding, T. P. & Seely, D. R. 1973. Basic wrench tectonics. *Bull. Am. Ass. Petrol. Geol.* **57**, 74–96.

Wilson, G. 1970. Wrench movements in the Aristarchus region of the Moon. *Proc. Geol. Ass.* **81**, 595–608.

Woodcock, N. H. & Robertson, A. H. F. 1982. Wrench and thrust tectonics along a Mesozoic–Cenozoic continental margin, Antalya complex, SW Turkey. *J. geol. Soc. Lond.* **139**, 147–163.